Mass-Preserving Motion Correction of PET: Displacement Field vs. Spline Transformation

Fabian Gigengack, Lars Ruthotto, Martin Burger,
Carsten H. Wolters, Xiaoyi Jiang, *Senior Member, IEEE,* and Klaus P. Schäfers

***Abstract*—In positron emission tomography (PET), motion due to the cardiac and respiratory cycle causes blurred images. Different approaches for motion correction in PET vary in the general concept (optical flow or image registration) or, e.g., in the discretization of motion. Given our mass-preserving transformation model, we evaluate different motion models in this work: dense displacement field (compute for each voxel an individual displacement) vs. spline transformation (i.e. free-form deformation). Thereby a focus is put on the parametrization of the spline transformations where we optimize the number of spline coefficients and the regularization parameter. We make a quantitative comparison of the motion estimates of the different motion models based on data of the established XCAT software phantom. For both motion models (displacement field (DF) and spline transformation (ST)) the registration results are evaluated by 1) the total processing time and 2) the Euclidean distance to the ground-truth vectors provided by the XCAT phantom. We found that the spline transformation model is superior to the displacement field strategy in terms of processing time and accuracy.**

***Index Terms*—motion correction, mass-preservation, image registration, spline transformation, hyperelastic regularization, PET**

I. Introduction

In positron emission tomography (PET), motion due to the cardiac and respiratory cycle causes blurred images. Various algorithms for motion correction in PET were recently developed [1], [2]. In this context, we proposed the incorporation of prior knowledge (preservation of mass) into the registration process with the Variational Algorithm for Mass-Preserving Image REgistration (VAMPIRE) [3], [4], [5].

The different approaches for motion correction in PET vary in the general concept (optical flow [2] or image registration [1], [3]) or, e.g., in the motion model. Given our mass-preserving transformation model [3], we evaluate in this work different motion models in the sense of [6]: dense displacement field (compute for each voxel an individual displacement) vs. spline transformation (i.e. free-form deformation). Thereby a focus is put on the parametrization of the spline transformations where we optimize the number of spline coefficients and the regularization parameter.

Based on the ground-truth motion vectors, provided by the established XCAT software phantom [7], we make a quantitative comparison of the motion estimates of the different motion models.

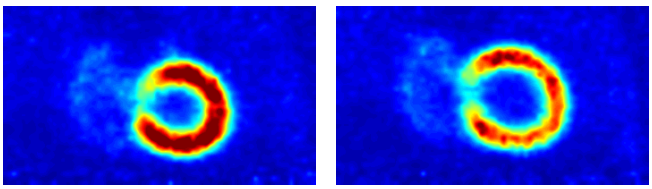

(a) Template image $\mathcal{T}$ (b) Reference image $\mathcal{R}$

Fig. 1. The template image $\mathcal{T}$ is registered to the reference image $\mathcal{R}$.

II. Materials and Methods

A. XCAT Phantom Data

Two gates with varying cardiac and respiratory phase are generated with the XCAT software phantom [7]: one template image $\mathcal{T}$, showing the systolic heart phase at maximum inspiration, and a reference image $\mathcal{R}$ in the diastolic heart phase at mid-expiration, see Fig. 2(a).

The simulated tracer uptake values were derived from a real ^{18}F-FDG patient scan [3]. The ideal images of the XCAT tool were blurred with a Gaussian kernel to simulate the partial volume effect (PVE) ($\mathrm{FWHM} \approx 3.85\,\mathrm{mm}$). The blurred images were forward projected into data space, where Poisson noise was simulated. In a final step, the sinograms were reconstructed with an EM algorithm [8], [9] which can be downloaded at [10].

The original images were cropped to a size of $80 \times 80 \times 44$ with a voxel size of $3.375\,\mathrm{mm}$.

B. VAMPIRE - *Variational Algorithm for Mass-Preserving Image REgistration*

A template image $\mathcal{T} : \Omega \to \mathbb{R}$ is registered onto an assigned reference image $\mathcal{R} : \Omega \to \mathbb{R}$, where $\Omega \subset \mathbb{R}^3$ is the image domain. This yields a transformation $y : \mathbb{R}^3 \to \mathbb{R}^3$

This work was partly funded by the Deutsche Forschungsgemeinschaft, SFB 656 MoBil (projects B2 and B3) and projects BU2327/2-1, JU445/5-1 and WO1425/1-1.

F. Gigengack is with the European Institute for Molecular Imaging (EIMI) and the Department of Mathematics and Computer Science, University of Münster, Germany.

L. Ruthotto is with the Institute of Mathematics and Image Computing (MIC), University of Lübeck, Germany.

M. Burger is with the Institute for Computational and Applied Mathematics, University of Münster, Germany.

C. H. Wolters is with the Institute for Biomagnetism and Biosignalanalysis, University of Münster, Germany.

X. Jiang is with the Department of Mathematics and Computer Science, University of Münster, Germany.

K. Schäfers is with the European Institute for Molecular Imaging (EIMI), University of Münster, Germany.

Corresponding author: fabian.gigengack@uni-muenster.de.

representing point-to-point correspondences between $\mathcal{T}$ and $\mathcal{R}$. To find y, the following functional has to be minimized

$$\min_y \ \mathcal{D}(\mathcal{M}^{\text{MP}}(\mathcal{T}, y),\ \mathcal{R}) + \alpha\, \mathcal{S}(y)\ . \tag{1}$$

$\mathcal{D}$ denotes the distance functional (sum-of-squared differences (SSD) in our case) and $\mathcal{M}^{\text{MP}}$ the mass-preserving transformation model

$$\mathcal{M}^{\text{MP}}(\mathcal{T}, y) := (\mathcal{T} \circ y) \cdot \det(\nabla y) = \mathcal{T}(y) \cdot \det(\nabla y)\ . \tag{2}$$

In the mass-preserving transformation model of VAMPIRE the template image $\mathcal{T}$ is transformed by interpolation on the deformed grid y with an additional multiplication by the volumetric change. $\mathcal{S}$ is the regularization functional.

For the parametric spline transformation, y is computed from a set of parameter w ($y = y(w)$). Hence, the functional in (1) is be optimized in w.

The implementation is based on the freely available FAIR toolbox [11] in MATLAB®. We use a multi-level strategy along with a Gauss-Newton optimization. The VAMPIRE code can be downloaded at [12]. Some time critical operations, like interpolation and regularization, were implemented matrix free and parallelized in C to keep memory usage to a minimum and to speedup the computation. All computations were evaluated on a quad-core 64-bit Linux machine with 2.50 GHz and 7.5 GB RAM.

C. Displacement Field (DF)

For the DF registration we performed a parameter search for the hyperelastic regularizer [13] parameter (vector) α by minimizing the error measure e in Equation (3).

D. Spline Transformation (ST)

For the ST we varied the regularization between hyperelastic and the internal FAIR regularization for splines (penalizing the norm of the coefficients) [11]. The parameters for hyperelastic regularization with ST were set to the same values as estimated for the hyperelastic DF registration since the same data with the same noise level is processed. The FAIR regularization was evaluated for different values, i.e., $\alpha \in \{5 \cdot 10^5, 10^6, 5 \cdot 10^6\}$. In addition, the optimal number of spline coefficients was part of the optimization. The image size was divided by a factor $s \in \{2, 4, 6, 8, 10, 12, 14, 16, 18\}$ to define the number of spline coefficients. Given an image size of $80 \times 80 \times 44$, the number of spline coefficients varies between $40 \times 40 \times 22$ ($s = 2$) and $4 \times 4 \times 2$ ($s = 18$). Given a voxel size of $3.375\,\text{mm}$, s can also be interpreted as putting every $s \cdot 3.375\,\text{mm}$ a spline coefficient. Consequently, the spacing of the coefficients ranges from $6.75\,\text{mm}$ ($s = 2$) to $60.75\,\text{mm}$ ($s = 18$).

III. RESULTS

For both motion models (DF and ST) the registration results are evaluated by 1) the total processing time and 2) the error measure

$$e(y, y_{GT}) := \frac{1}{|\Omega|} \int_\Omega \|y(x) - y_{GT}(x)\| dx\ . \tag{3}$$

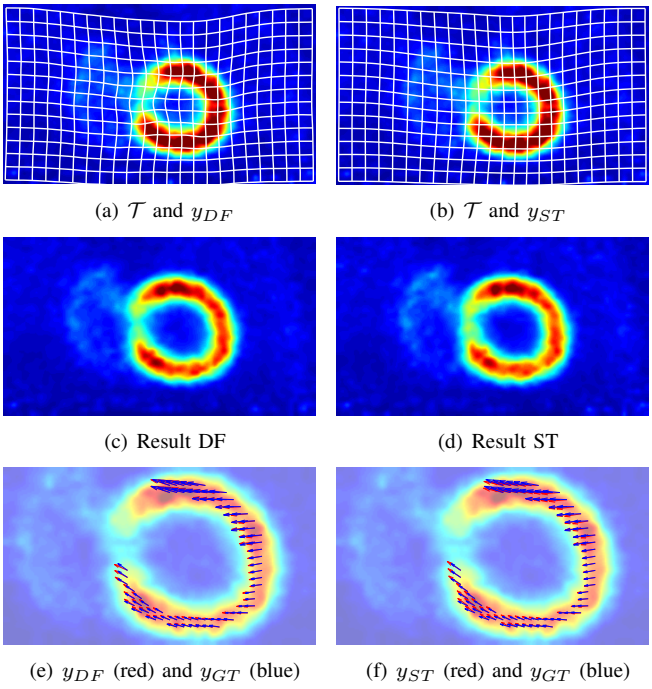

(a) $\mathcal{T}$ and y_{DF} (b) $\mathcal{T}$ and y_{ST}

(c) Result DF (d) Result ST

(e) y_{DF} (red) and y_{GT} (blue) (f) y_{ST} (red) and y_{GT} (blue)

Fig. 2. $\mathcal{T}$ (Fig. 1(a)) is registered to $\mathcal{R}$ (Fig. 1(b)) once with a displacement field (DF) ((a) and (c)) and once with a spline transformation (ST) model ($s = 10$, $\alpha = 5 \cdot 10^6$) ((b) and (d)). A magnification with a comparison of the estimated vectors and the ground-truth vectors is shown in (e) and (f).

As only regions with significant tracer uptake provide information for the registration process, the error evaluation is consequentially restricted to the left ventricle where a high uptake is simulated.

Displacement Field vs. Spline Transformation

For the DF an accuracy of $1.96\,\text{mm}$ could be achieved. The VAMPIRE algorithm terminated after $326\,\text{s}$. The resulting grid y is overlaid on template image in Fig. 2(a). The image after applying the mass-preserving transformation can be seen in (c). A comparison of the estimated and the ground-truth transformation is given in (f).

The results of the ST evaluation can be seen in Fig. 3. The factor s is plotted against the ground-truth distance e of the estimated motion vectors in (a) and against the total processing time in (b). In addition to the spline results, a solid black horizontal line is plotted which represents the DF result.

IV. DISCUSSION AND CONCLUSION

For ST and all regularization parameters settings an optimal number of spline coefficients of $8 \times 8 \times 4$ ($s = 10$) was found. This represents a spacing of $3.375\,\text{cm}$ for the spline coefficients.

For $s = 10$ hyperelastic regularization ($e = 1.47\,\text{mm}$) and FAIR regularization with $\alpha = 5 \cdot 10^5$ ($e = 1.56\,\text{mm}$), $\alpha = 10^6$ ($e = 1.52\,\text{mm}$), and $\alpha = 5 \cdot 10^6$ ($e = 1.59\,\text{mm}$) lead to comparable accuracies. With the given voxel size of $3.375\,\text{mm}$ all these values represent a subvoxel accuracy. The processing time of hyperelastic regularization ($79\,\text{s}$) was longer compared to the times for these three α-values ($45\,\text{s}$, $42\,\text{s}$, and

TABLE I
DETAILED COMPARISON OF THE DISPLACEMENT FIELD AND SPLINE TRANSFORMATION RESULTS. FOR ST ONLY THE VALUES FOR $s = 10$ (OPTIMAL COEFFICIENT FACTOR) ARE SHOWN. BEST RESULTS ARE LABELED IN GREEN.

	Displacement Field (Fig. 2(a), (c), (e))	**Spline Transform.**	**Spline Transform.**	**Spline Transform.**	**Spline Transform.** (Fig. 2(b), (d), (f))
Spline coefficient factor	–	$s = 10$	$s = 10$	$s = 10$	$s = 10$
Regularization scheme	hyperelastic	hyperelastic	$\alpha = 5 \cdot 10^5$	$\alpha = 10^6$	$\alpha = 5 \cdot 10^6$
Error measure $e(y, y_{GT})$	1.96 mm	1.47 mm	1.56 mm	1.52 mm	1.59 mm
Processing time t	326 s	79 s	45 s	42 s	28 s

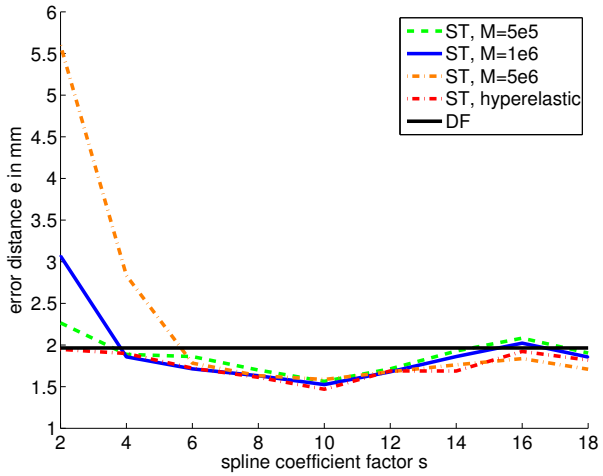

(a) Error measure e against coefficient factor s

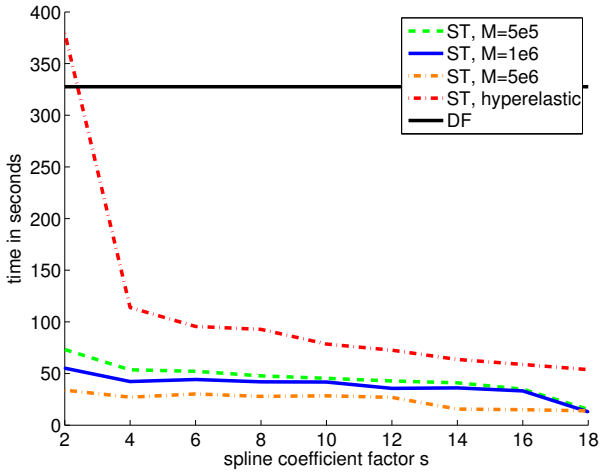

(b) Time t against coefficient factor s

Fig. 3. The ground-truth distance e and the processing time is plotted against the spline coefficient factor s. The different regularization variants are shown for the spline transformation model. The solid black lines represents the result of the displacement field computation.

28 s) for ST. As a short processing time is desired the optimal regularization is $\alpha = 5 \cdot 10^6$.

In contrast to the FAIR regularization, hyperelastic regularization [13] guarantees diffeomorphic (i.e. invertible) transformations which should give preference to the hyperelastic regularization. However, throughout all computations in this paper, including the FAIR regularized registrations, the determinant of the transformation's Jacobian was positive and finite, indicating invertibility.

It might further be interesting to make a comparison of the results in this paper and the displacement field strategy while stopping at different levels in the multi-level pyramid. It might be promising to stop at the last but one resolution level and to prolongate the grid to the final resolution. This might further stabilize the methods' robustness against noise and save computation time while having a sufficient accuracy.

In conclusion, comparing the ST results with the DF results (see Fig. 3) reveals that the spline transformation model ($s = 10$ and $\alpha = 5 \cdot 10^6$, shown in Fig. 2(b), (d), (f)) is superior to the displacement field strategy in terms of processing time (ST: 28 s vs. DF: 326 s) and accuracy (ST: 1.59 mm vs. DF: 1.96 mm).

V. ACKNOWLEDGMENTS

The authors would like to thank Thomas Kösters for providing his reconstruction software EMRECON used for reconstruction. Especially, we thank Jan Modersitzki for his advise regarding the implementation and for making his FAIR toolbox freely available.

REFERENCES

[1] W. Bai and M. Brady, "Motion correction and attenuation correction for respiratory gated PET images," *IEEE Trans. Med. Imag.*, vol. 30, no. 2, pp. 351–365, 2011.
[2] M. Dawood, F. Büther, X. Jiang, and K. Schäfers, "Respiratory motion correction in 3-D PET data with advanced optical flow algorithms," *IEEE Trans. Med. Imag.*, vol. 27, no. 8, pp. 1164–1175, 2008.
[3] F. Gigengack, L. Ruthotto, M. Burger, C. Wolters, X. Jiang, and K. Schäfers, "Motion correction in dual gated cardiac pet using mass-preserving image registration," *IEEE Trans. Med. Imag.*, In press.
[4] F. Gigengack, L. Ruthotto, M. Burger, C. Wolters, X. Jiang, and K. Schaefers, "Motion correction of cardiac PET using mass-preserving registration," in *NSS/MIC, IEEE*, 2010.
[5] L. Ruthotto, "Mass-preserving registration of medical images," German Diploma Thesis (Mathematics), Institute for Computational and Applied Mathematics, University of Münster, march 2010.
[6] M. Blume, A. Keil, N. Navab, and M. Rafecas, "Joint reconstruction of image and motion for PET: Displacement fields versus a B-spline motion model," in *NSS/MIC Conference Record, IEEE*, 2010, pp. 3506–3508.
[7] W. Segars, M. Mahesh, T. Beck, E. Frey, and B. Tsui, "Realistic CT simulation using the 4d XCAT phantom," *Med. Phys.*, vol. 35, no. 8, pp. 3800–3808, 2008.
[8] T. Kösters, K. Schäfers, and F. Wübbeling, "EMRECON: An expectation maximization based image reconstruction framework for emission tomography data," in *NSS/MIC Conference Record, IEEE*, 2011.
[9] T. Kösters, "Derivation and analysis of scatter correction algorithms for quantitative positron emission tomography," Ph.D. dissertation, University of Münster, 2010.
[10] [Online]. Available: http://emrecon.uni-muenster.de
[11] J. Modersitzki, *FAIR: Flexible Algorithms for Image Registration*. Philadelphia: SIAM, 2009.

[12] [Online]. Available: http://vampire.uni-muenster.de
[13] M. Droske and M. Rumpf, "A variational approach to nonrigid morphological image registration," *SIAM J. Appl. Math.*, vol. 64, no. 2, pp. 668–687, 2003.